Localization of Cholesterol and Fatty Acid in a Model Lipid Membrane: A Neutron Diffraction Approach

E. H. Mojumdar,[†] D. Groen,[†] G. S. Gooris,[†] D. J. Barlow,[‡] M. J. Lawrence,[‡] B. Deme,[§] and J. A. Bouwstra[†*]
[†]Leiden/Amsterdam Center for Drug Research, Department of Drug Delivery Technology, Gorlaeus Laboratories, University of Leiden, Leiden, the Netherlands; [‡]Pharmaceutical Science Division, King's College London, London, United Kingdom; and [§]Institut Laue-Langevin, Grenoble, France

ABSTRACT The intercellular lipid matrix of the skin's *stratum corneum* serves to protect the body against desiccation and simultaneously limits the passage of drugs and other xenobiotics into the body. The matrix is made up of ceramides, free fatty acids, and cholesterol, which are organized as two coexisting crystalline lamellar phases. In studies reported here, we sought to use the technique of neutron diffraction, together with the device of isotopic (H/D) substitution, to determine the molecular architecture of the lamellar phase having a repeat distance of 53.9 ± 0.3 Å. Using hydrogenous samples as well as samples incorporating perdeuterated (C24:0) fatty acids and selectively deuterated cholesterol, the diffraction data obtained were used to construct neutron scattering length density profiles. By this means, the locations within the unit cell were determined for the cholesterol and fatty acids. The cholesterol headgroup was found to lie slightly inward from the unit cell boundary and the tail of the molecule located 6.2 ± 0.2 Å from the unit cell center. The fatty acid headgroups were located at the unit cell boundary with their acyl chains straddling the unit cell center. Based on these results, a molecular model is proposed for the arrangement of the lipids within the unit cell.

INTRODUCTION

The outermost layer of the skin, the *stratum corneum* (SC), protects the body from desiccation, and simultaneously controls the penetration of drugs and other molecules into the body (1). The SC consists of dead flattened cells, the corneocytes, embedded in a lipid matrix composed of lipid lamellae. The corneocytes are surrounded by a densely cross-linked protein layer, the cornified envelope. This protein layer reduces the partitioning of substances into the cells and therefore redirects the penetration of substances along the intercellular lipid matrix (2,3). The architecture of the SC is often described as a brick-and-mortar structure, in which the corneocytes are the bricks and the intracellular lipid matrix is the mortar (4).

The composition of the SC lipid matrix is unique. The main lipid components are ceramides (CERs), cholesterol (CHOL), and free fatty acids (FFAs) in an approximately equimolar ratio (5). Small amounts of cholesterol sulfate and cholesterol esters are also present in the SC (6–8). CERs are the key components and play a crucial role in the molecular organization in the SC (9,10). So far, 12 CER subclasses have been identified in the human SC (11–14).

In previous studies, it has been reported that the majority of SC lipids are organized to form two coexisting crystalline lamellar phases, referred to as the long periodicity phase (LPP) with a repeat distance of ~130 Å, and the short periodicity phase (SPP), with a repeat distance of ~60 Å (15–19). In additional studies, lipid mixtures were used to examine the lipid phase behavior. These mixtures were prepared with either CERs isolated from SC (20,21) or synthetic CERs mixed with CHOL and various FFAs (22–25). By selecting the proper preparation method and composition, these mixtures mimic the SC lipid phase behavior very closely, giving two crystalline lamellar phases similar to those found in SC (21,24,26,27). Both phases are formed in mixtures containing just five CER subclasses (see Fig. S1 in the Supporting Material). As far as the LPP is concerned, electron density calculations from x-ray diffraction profiles have shown that this is not a single bilayer structure, very different from most phospholipid lamellar phases (28,29). In the case of the SPP, the shorter repeat distance indicates an arrangement of the lipids in bilayers.

To obtain in-depth information on the skin barrier, not only the lipid phase behavior but also information about the molecular arrangement of CERs, CHOL, and FFAs within the lamellar phases is important. To date, most research on the molecular arrangement of CHOL, CER, and FFA mixtures has been performed using simplified mixtures prepared from only 3–5 lipid components. Although very valuable information has been obtained on the arrangement of the FFA in these systems, the lipid phase behavior of these simplified mixtures is quite different from that in SC (25,30,31).

In previous studies, we have demonstrated that CER:CHOL:FFA mixtures in the absence of acyl CER (a CER with a very long fatty-acid chain; see Fig. S1) form only the SPP with a repeat distance of 54 Å (32). Using neutron diffraction together with isotopic substitution, we have embarked upon a series of investigations to determine the arrangement of the CER, CHOL, and FFA within this model SC system. In our first such studies, we showed that the most

Submitted April 18, 2013, and accepted for publication July 1, 2013.

*Correspondence: bouwstra@chem.leidenuniv.nl

Editor: Huey Huang.

0006-3495/13/08/0911/8 $2.00

http://dx.doi.org/10.1016/j.bpj.2013.07.003

abundant CER subclass, CER nonhydroxy sphingosine (CER NS), is symmetrically arranged within the SPP unit cell (32). In the studies reported here, we extend this work to examine the molecular arrangement of the other two main subclasses within the SPP, namely CHOL and FFAs. Here we selected the FFA with a chain length of 24 carbon atoms (FA C24:0) also known as lignoceric acid. CHOL molecules were used either deuterated in the headgroup or deuterated in the tail of the molecule, while the FFA C24:0 was perdeuterated. Using neutron diffraction, we determined the localization of FFA in the SPP, and the localization of the CHOL headgroup and tail.

MATERIALS AND METHODS

Materials

Five subclasses of synthetic CERs were used for our studies. These were a nonhydroxyl acyl chain (C24) linked to a sphingosine chain length C18 referred to as CER NS (C24), a nonhydroxy acyl chain (C24 or C16) linked to phytosphingosines referred to as CER NP (C24) and CER NP (C16), ceramide α-hydroxy linked to a sphingosine base referred to as CER AS (C24), and an α-hydroxy acyl chain (C24) linked to a phytosphingosine referred to as CER AP (C24). The number between parentheses indicates the number of carbon atoms present in the acyl chain of the CERs. All the CERs were kindly provided by Evonik (Essen, Germany). The molecular architecture of these CERs is provided in Fig. S1. The CHOL with head deuterated in the positions 2, 3, and 4 (total of six deuterium) and tail deuterated in the positions 25, 26, and 27 (total of seven deuterium) were obtained from Larodan (Malmö, Sweden). The FFAs with chain lengths of C16:0, C18:0, C20:0, C22:0, C23:0, C24:0, and C26:0 and CHOL and deuterated water were purchased from Sigma-Aldrich Chemie (Schnelldorf, Germany). Deuterated C24:0 FFA was obtained from Arc Laboratories (Apeldoorn, The Netherlands). The structures of deuterated CHOL and FFA C24:0 are provided in Fig. S2. Silicon substrates for the neutron diffraction studies were cut from a wafer (P-type, contains Boron as dopant, face aligned on the (110) crystal plane, thickness 380 $\pm$ 10 μm) obtained from Okmetic (Vantaa, Finland). All solvents used were of analytical grade and supplied by Labscan (Dublin, Ireland). The water was of Millipore (Billerica, MA) quality.

Sample preparation

The model lipid membranes consisted of CERs, CHOL, and FFAs in an equimolar ratio. The CER subclasses were mixed in a molar ratio of 60:19:5:11:6 for CER NS C24: CER NP C24: CER AS C24: CER NP C16: CER AP C24. This ratio resembles very closely the CER composition in the pig SC (20), except that acyl CERs are not present. In all these CERs, the sphingoid base has a chain length of C18. The FFA composition is C16:0, C18:0, C20:0, C22:0, C23:0, C24:0, and C26:0 in a molar ratio of 1.8:4.0:7.7:42.6:5.2:34.7:4.1. This composition is based on the FFA chain-length distribution reported for human SC (33). For preparing the mixture with a perdeuterated FFA, the protonated FFA C24:0 was replaced by its perdeuterated counterpart. Four different lipid model membrane systems were prepared:

System I, with the protonated lipids only;
System II, with the cholesterol headgroup deuterated;
System III, with the cholesterol tail deuterated; and
System IV, with FFA C24 perdeuterated.

For preparing the mixtures, the lipids were dissolved in chloroform/methanol (2:1 v/v) solution at 10 mg/mL. The lipids were subsequently sprayed on a silicon substrate in an area of 1.2 $\times$ 4.0 cm^2 using a Camag Linomat IV sample applicator (Muttenz, Switzerland). The spraying rate was set to 5 μL/min. During spraying, the solvent was evaporated by a gentle flow of nitrogen gas. The total amount of lipid sprayed on the substrate was ~10 mg.

After spraying, the lipid films were inserted in a substrate aluminum chamber to facilitate a homogenous temperature environment. Argon gas was added in the chamber to avoid lipid oxidation at elevated temperatures. The lipid mixture was equilibrated at ~70°C for ~10 min, which is close to the melting temperature of the mixture. The samples were then cooled down to room temperature. The same equilibration procedure was applied for all four lipid model mixtures. After equilibration, the samples were hydrated with D_2O/H_2O buffer at 100% relative humidity (RH) for ~15 h at 37°C before the neutron diffraction measurements.

To determine the phase signs of the structure factors, the samples were hydrated at three different D_2O/H_2O concentrations: 8/92, 33/67, and 100/0 (v/v) for CHOL and 8/92, 50/50, and 100/0 (v/v) for FFA. After measuring at a particular D_2O/H_2O concentration, the samples were allowed to hydrate for ~12 h, 37°C, at a different D_2O/H_2O concentration at 100% RH.

Neutron diffraction

Neutron diffraction experiments were performed on the D16 cold neutron diffractometer of the Institut Laue-Langevin (Grenoble, France). The primary white beam was reflected by a focusing highly-ordered pyrolytic graphite monochromator to achieve a wavelength of 4.75 Å. The wavelength spread of the highly-ordered pyrolytic graphite monochromator is 1%. The sample-to-detector distance was 80 cm and all the samples were measured in the reflection mode. The samples were mounted on a goniometer placed in an aluminum chamber. The temperature of the chamber was maintained at 25°C throughout the measurements. During the sample measurements, the bottom of the chamber was filled with the same D_2O/H_2O concentrations as used for hydrating the sample, to maintain a 100% RH and a constant D_2O/H_2O. The measurement time per sample varied between 6 and 9 h, depending on the signal/noise. The neutron scattering density was recorded by a position-sensitive two-dimensional ^{3}He detector (320 $\times$ 320-mm area with a spatial resolution of 1 $\times$ 1 mm).

Data refinement

A water calibration measurement was used to correct for the intensity differences of the detector surface. An empty chamber was measured as a background and subtracted from each measurement to increase the signal/noise. For data analysis, the Institut Laue-Langevin's in-house software LAMP was used (34). The two-dimensional detector data were integrated in the vertical direction, which results in a one-dimensional diffraction pattern of scattering intensities (I) as a function of the scattering angle (2θ). The scattering angle 2θ is converted to the scattering vector q as follows:

$$q = \frac{4.\pi.\sin\theta}{\lambda}. \quad (1)$$

In this equation, θ is the Bragg angle, λ is the wavelength of the neutron beam, and h is the diffraction order. The repeat distance d of the unit cell was calculated from the positions of a series of equidistant peaks attributed to the lamellar phase (q_h) by

$$d = \frac{2.\pi.h}{q_h}. \quad (2)$$

During the measurements, the sample was rotated in steps of 0.1° from 0 to 26° to cover all five diffraction orders, and detector images were taken at each step. We integrated the high-intensity part of the sample peak around the Bragg angle because there the lamellae are oriented parallel

to the silicon substrate. To this purpose we used two data points before the Bragg angle, the Bragg angle point, and two data points after the Bragg angle for each diffraction order ($\Omega = -0.2, -0.1, 0.0, +0.1, +0.2$). The mosaic spread of the peaks were determined from the neutron rocking curves and was ~1.0° with a full width at half-maximum of the peaks of ~0.3°. This indicates the data points we choose for integration were sufficiently broad to cover the entire peak. Summing all pixel intensities for those five data points and averaging them results in a high signal/noise for each diffraction order. This procedure was applied to the diffraction orders of all four model membranes. The structure factor amplitude $|F_h|$ of each diffraction peak was then calculated from the average pixel intensity (I_h) by

$$|F_h| = A_h\sqrt{L.I_h}. \quad (3)$$

The Lorentz correction (L) for our type of sample system is 2 sin θ cos θ. The appropriate values were calculated for all the systems and applied to correct for the intensities. The value A_h is the correction factor for sample absorption, which was calculated using the following formula (35):

$$A_h = \frac{\sin\theta}{2\mu L}\left(1 - e^{\frac{-2\mu L}{\sin\theta}}\right). \quad (4)$$

Here μ represents the linear attenuation coefficient and L is the thickness of the lipid film. In previous studies the lipid density for the mixture was determined at ~0.873 g/cm^3 (32). Taking into account the water molecules used at different D_2O/H_2O for preparing the various samples and assuming two water molecules per lipid molecule as determined in our previous study (32), the densities of the various samples were recalculated and provided in Table 1. From the amount of lipid material, the area of spraying (4.8 cm^2), and the density of our lipid membranes, a lipid membrane thickness of ~24 μm was obtained. The attenuation coefficients were calculated using the wavelength of the neutrons in combination with the lipid density and the chemical composition of the lipid films (NIST Center for Neutron Research (36)) and are presented in Table 1. Because both the lipid thickness and the attenuation coefficient were calculated from the lipid densities, they actually cancel out in the absorption correction. As a result, any uncertainty or controversy about the densities does not affect the absorption correction. The error in the structure factors by D_2O/H_2O exchange were calculated from deviation of the fitted regression line and shown in Table 2. These errors reflected the true variation of calculated structure factors from the fitted regression line.

If we consider our SPP unit cell as centrosymmetric, the structure factor phase signs would be either plus (+) or minus (−). In such a case, the structure factor amplitudes change linearly with increasing D_2O/H_2O (35). Because we assume that the water is located near the headgroups at the boundaries of the unit cell, the phase signs of the structure amplitudes of water are −, +, −, +, and − for the five orders measured (an explanation is given in the Supporting Material for the water-phase sign determination).

TABLE 1 Lipid densities and linear attenuation coefficients for different model membranes at different values of D_2O%

	Model membrane	D_2O%	Density, (g/cm^3)	Attenuation coefficient (cm^{-1})
Protonated	System I	8	0.922	5.840
		8	0.922	5.624
CHOL head deuterated	System II	33	0.954	5.720
		100	1.031	5.913
		8	0.922	5.588
CHOL tail deuterated	System III	33	0.954	5.683
		100	1.031	5.874
		8	0.922	4.374
FFA C24 perdeuterated	System IV	50	0.961	4.630
		100	1.031	4.892

In addition, the water layer structure factors are defined as the structure factors at 100% D_2O minus the structure factors at 8% D_2O. Using this information, the structure factor phase signs for both protonated and deuterated samples could be determined from the linear plot of the structure factors versus measures of D_2O/H_2O. This was done in such a way that the difference between 100% D_2O and 8% D_2O corresponds to the correct phase sign for the water layer structure factor at that particular diffraction order. A more detailed description is given elsewhere (35,37,38).

Subsequently, the scattering length density (SLD) profile across the bilayer $\rho(x)$ was calculated by Fourier reconstructions,

$$\rho(x) = F_0 + 2\sum_{h=1}^{h_{max}} F_h \cos\left(\frac{2.\pi.h.x}{d}\right), \quad (5)$$

where x is the distance normal to the bilayer surface and $x = 0$ is the center of the bilayer.

The first term of the equation F_0 describes the average scattering density per unit volume and must be calculated to put the data on an absolute scale. The F_0 was calculated using the chemical composition and the mass density of the sample (39,40). The data were then put on a relative-absolute scale (41–43) using the known neutron SLDs of deuterium and hydrogen to scale the differences in such a way that the area differences between the SLDs should be equal to the SLD of the deuterium label (for example, a seven-deuterium difference in the case of CHOL tail deuterated). The difference density profile was then constructed by subtracting the protonated profile from the deuterated profile.

RESULTS

Four different model membrane systems were measured with neutron diffraction. The diffraction pattern of each of the four samples showed five diffraction orders. A typical three-dimensional plot of a diffraction pattern is depicted in Fig. S3. The one-dimensional diffraction pattern of intensity as a function of q is provided in Fig. 1 for all the deuterated systems at 100% D_2O contrast. The sharp peaks in the diffraction pattern indicate a highly preferred orientation of the lamellae parallel to the support. In addition, from the pattern we concluded that only one lamellar phase was present in the sample together with crystalline CHOL. The CHOL peaks did not interfere with the peaks attributed to the lamellar phase. From the position of the different diffraction orders of the lamellar phase, the repeat distance of the unit cell was calculated for all the different model systems using Eqs. 1 and 2. The repeat distance as well as the uncertainty was calculated by a least-square fitting of all the diffraction orders for all the systems used in our study and are provided in Table 2. The mean repeat distance of all the samples was calculated to be 53.9 ± 0.3 Å.

In previous studies, it was estimated that only two water molecules per lipid molecule are incorporated in the SPP unit cell (32). The low level of water results in a moderate increase of signal/noise in the diffraction pattern when increasing the D_2O/H_2O. However, despite the low water affinity of the lipids forming the SPP, the contrast was sufficient to discriminate between the protonated and deuterated model membrane systems.

The structure factor amplitudes and absorption correction factors for different diffraction orders were calculated using

TABLE 2 Repeating unit of the SPP lamellae (*D*), relative structure factors with their corresponding phase signs (*F*), and standard errors and the absorption correction factors (*A*) for all the different model systems

	D_2O%	*D* (Å)	*F*1	*A*1	*F*2	*A*2	*F*3	*A*3	*F*4	*A*4	*F*5	*A*5
Protonated	8	54.3 ± 0.1	−26.8 ± 1.3	1.2	19.2 ± 0.6	1.1	−12.3 ± 0.2	1.1	10.2 ± 0.4	1.0	−5.1 ± 0.4	1.0
	8	53.8 ± 0.2	−33.1 ± 1.2	1.2	22.1 ± 0.7	1.1	−10.6 ± 0.7	1.1	5.4 ± 0.7	1.0	−2.9 ± 0.2	1.0
CHOL head deuterated	33	53.4 ± 0.3	−44.2 ± 1.6	1.2	28.6 ± 0.9	1.1	−16.4 ± 0.9	1.1	10.6 ± 0.9	1.0	−3.5 ± 0.3	1.0
	100	53.8 ± 0.3	−64.2 ± 0.4	1.2	40.3 ± 0.3	1.1	−25.9 ± 0.3	1.1	19.31 ± 0.2	1.0	−7.0 ± 0.1	1.0
	8	54.1 ± 0.3	−26.3 ± 0.8	1.2	21.9 ± 0.1	1.1	−22.3 ± 0.6	1.1	4.6 ± 0.3	1.0	−14.6 ± 0.1	1.0
CHOL tail deuterated	33	53.8 ± 0.3	−37.6 ± 1.1	1.2	28.7 ± 0.1	1.1	−30.6 ± 0.8	1.1	8.6 ± 0.4	1.0	−18.3 ± 0.1	1.0
	100	53.8 ± 0.3	−61.2 ± 0.3	1.2	46.3 ± 0.1	1.1	−48.4 ± 0.2	1.1	21.4 ± 0.1	1.0	−27.9 ± 0.1	1.0
	8	54.1 ± 0.2	−36.9 ± 0.7	1.1	26.1 ± 0.5	1.1	−08.4 ± 0.5	1.0	13.9 ± 0.1	1.0	−04.6 ± 0.5	1.0
FFA C24 perdeuterated	50	54.1 ± 0.3	−40.2 ± 1.4	1.1	30.2 ± 0.9	1.1	−11.4 ± 0.9	1.0	17.2 ± 0.2	1.0	−08.9 ± 0.9	1.0
	100	53.9 ± 0.3	−48.5 ± 0.6	1.1	38.1 ± 0.4	1.1	−18.0 ± 0.4	1.0	22.1 ± 0.1	1.0	−11.1 ± 0.4	1.0

Eqs. 3 and 4. For determining the phase signs of the amplitudes of the different diffraction orders, the contrast variation method was used. Our studies showed that the structure of the unit cell was centrosymmetric because the structure factors changed linearly with increasing D_2O/H_2O (35). Assuming the water is at the boundary of the unit cell giving the water phase signs (−, +, −, +, −), the phase signs of the various diffraction orders of the SPP were then calculated keeping the difference between the structure factors of 8% D_2O and 100% D_2O in agreement with the correct phase signs for the water structure factors. Fig. 2 displays the linear relationship between the structure factors and the D_2O%. The corresponding structure factor amplitudes are provided in Table 2.

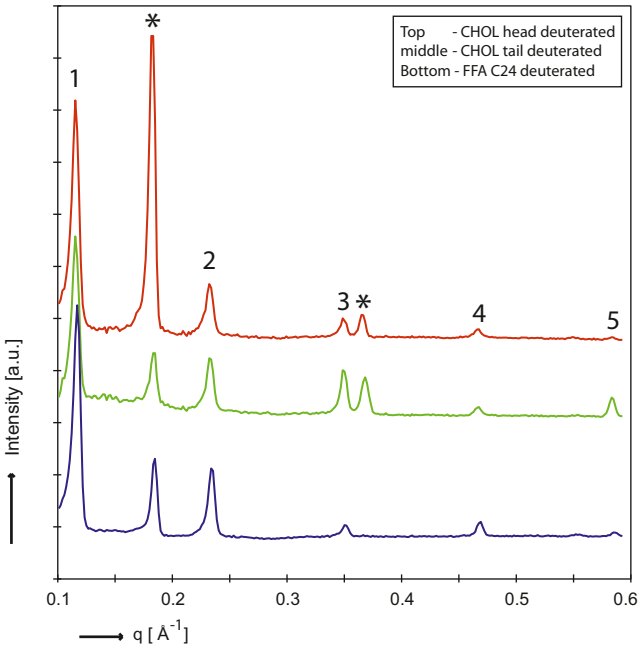

FIGURE 1 One-dimensional neutron diffraction plot of the SPP model membrane systems prepared with deuterated lipids and hydrated at 100% D_2O. The five different diffraction orders of the SPP unit lamellae are indicated by Arabic numerals and the CHOL peaks by means of asterisks. (*Top*) CHOL headgroup deuterated curve; (*middle*) CHOL tail deuterated curve; and (*bottom*) FFA C24 deuterated curve.

Using the calculated phase signs and structure factor amplitudes, the neutron SLD profiles were calculated using Eq. 5. The SLDs constructed at 8% D_2O are presented in Fig. 3. The difference density profiles for the deuterated CHOL and for the perdeuterated FFA molecule were obtained by subtracting the density profile for the fully hydrogenous system (System I) either from the profile for System II (with the deuterated cholesterol headgroup moiety), or from the profile for System III (with the deuterated tail region of CHOL), or from the profile for System IV (with the deuterated FFA). The difference density profiles (Fig. 4 *A*) clearly indicate that the CHOL headgroup is located slightly inwards from the unit cell boundary, with the CHOL tail 6.2 ± 0.2 Å from the unit cell center, while the FFA chain straddles the center of the unit cell, indicating a partial interdigitation of the fatty acyl chains (Fig. 4 *B*).

DISCUSSION

The aim of our study was to provide insight into the arrangement of the lipids within the repeating unit of the SPP present in human SC. Using x-ray diffraction it is possible to obtain information on the electron density profile of the unit cell. However, x-ray diffraction is limited in obtaining information on the localization of the lipid subclasses within the unit cell. Therefore, it was decided to perform neutron diffraction studies using contrast variation. This allowed us to localize the deuterated lipid moieties within the unit cell. In this study, we focused on the localization of CHOL and FFAs in the unit cell of the SPP. To avoid any overlapping diffraction peaks of the LPP and SPP, lipid mixtures without acyl CERs were used, preventing the formation of the LPP. The model lipid systems that we prepared formed oriented stacks of lamellar phase with a mean repeat distance of 53.9 ± 0.3 Å. Five different diffraction orders were measured in the scattering profiles of all four model systems. Two additional peaks attributed to the crystalline CHOL were also observed that did not interfere with the reflections attributed to the SPP. Recently, we observed that CHOL molecules are fully incorporated in the unit cell of the SPP until a molar ratio of 1:0.5:1 for CER/CHOL/FFA mixtures without the formation of phase-separated

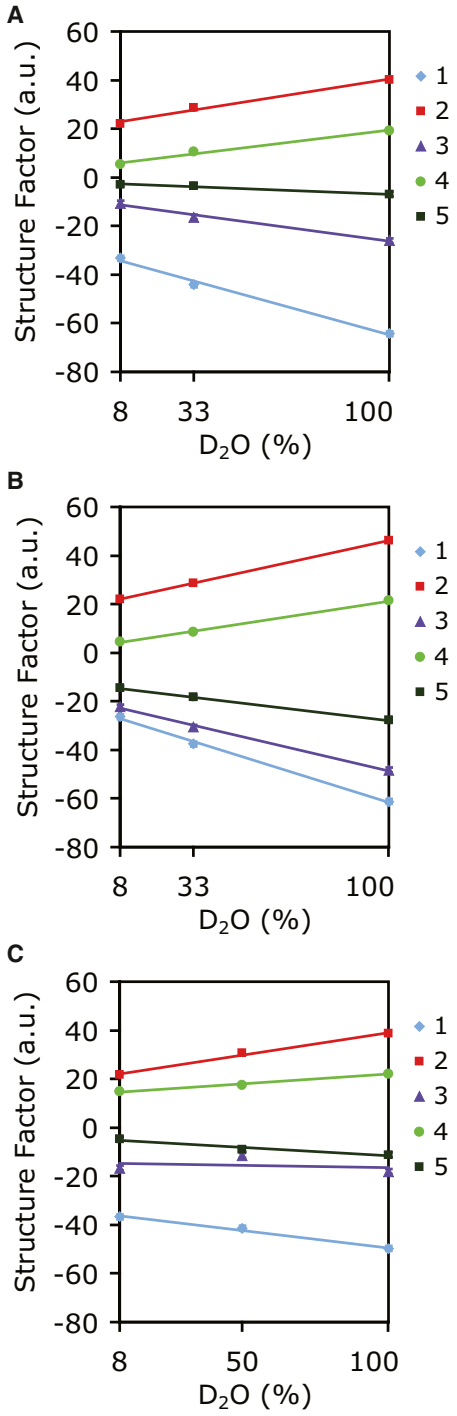

FIGURE 2 Relative structure factors of all the five different diffraction orders of the lipid membranes indicating their corresponding phase assignment measured as a function of D_2O/H_2O exchange ratio. The different numbers in the plots indicate the different diffraction orders. (*A*) System II with cholesterol head deuterated. (*B*) System III with cholesterol tail deuterated. (*C*) System IV with FFA C24 deuterated.

crystalline CHOL (E.H. Mojumdar, G.S. Gooris, and J.A. Bouwstra, unpublished data) obtained with an incremental of 0.1 CHOL molar ratio. A further increase in the CHOL level led to an equimolar ratio as observed in human SC

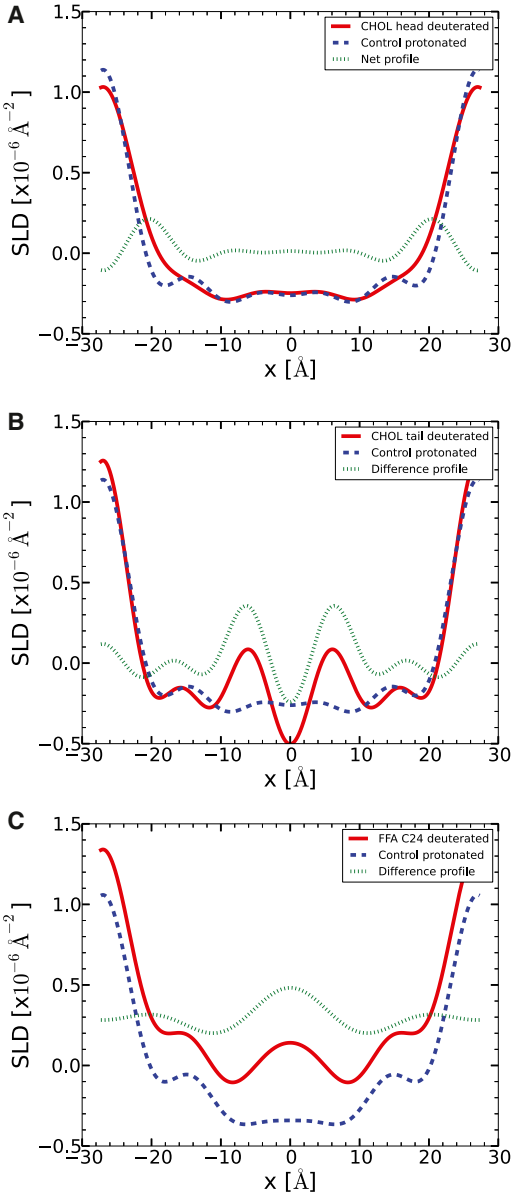

FIGURE 3 Neutron scattering length density (SLD) profiles of model lipid membranes in the direction normal to the unit cell surface. (*A*) System II with CHOL head deuterated; (*B*) System III with CHOL tail deuterated; and (*C*) System IV with FFA C24 deuterated. (*Dashed lines*, *blue curves*) Profiles of the protonated samples. (*Solid lines*, *red curves*) Profiles of the deuterated samples. (*Dotted lines*, *green curves*) Difference profiles between the deuterated and protonated samples; also shows the position of the deuterated CHOL and FFA C24 in the SPP unit cell. The calculated SLDs have a spatial resolution of ~5.4 Å and contain features based on the molecular position of the lipid materials.

results in phase-separated crystalline CHOL (5). Therefore, in the equimolar CER/CHOL/FFA used in this study, CHOL is partially incorporated in the lamellar phase and partially phase-separated (15,16,44). The reasons we chose to prepare equimolar mixtures are:

1. To mimic the native SC situation as closely as possible; and

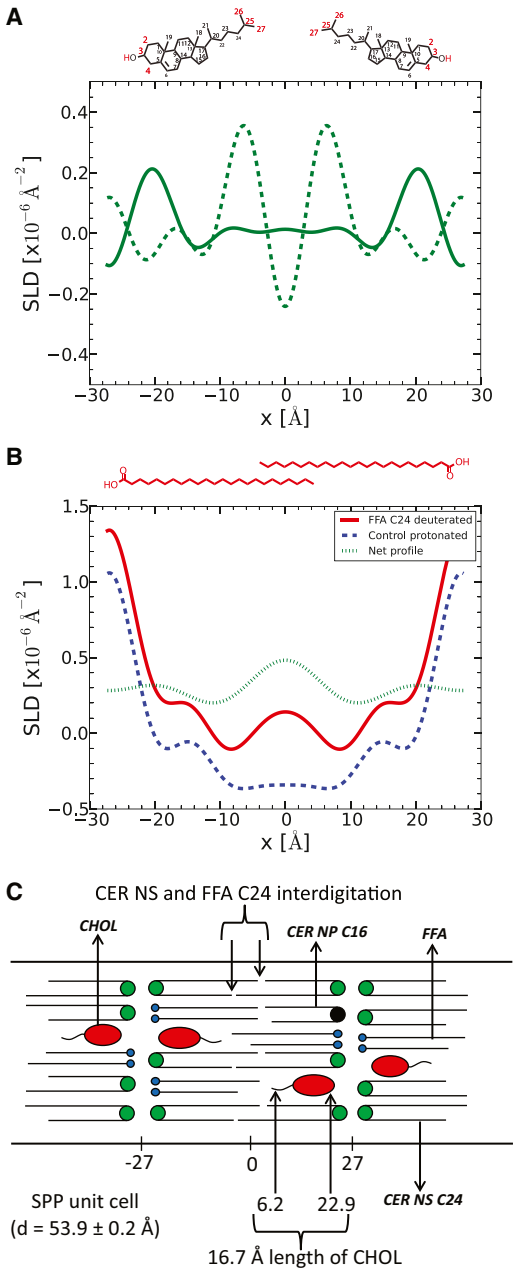

FIGURE 4 (*A*) The difference profiles in the scattering length density of the system with CHOL headgroup deuterated (*solid line*) and CHOL tail deuterated (*dashed line*, *green*). Deuterated CHOL molecules are also depicted showing their position in the SPP unit cell. (*B*) SLD profiles and schematic of the FFA C24 position in the SPP unit cell revealing the molecular position and overlapping of the FFA C24 and (*C*) a proposed molecular model of the SPP unit cell based on the positions of CER NP C16, CHOL, FFA, and CER NS determined earlier.

2. To confirm the knowledge from the previous unpublished data that 0.5 is the maximum level of CHOL in the lamellar phase, providing sufficient information to validate our absolute scaling.

Experimental studies and simulations have shown that CHOL has a much higher affinity for saturated acyl chains than for unsaturated ones (39,45), which may contribute to the presence of substantial levels of CHOL in the crystalline lipid lamellae.

CHOL positioning

Based on the density profiles for the systems containing the deuterated CHOL head and tail groups, the sterol molecules within the SPP are calculated to span a region of ~16.7 ± 0.3 Å thickness, indicating that the molecules must be fully extended and organized perpendicular to the layer plane. (Note that the dip at the center of the SLD profile for the tail-deuterated CHOL is an artifact arising from its truncation in the Fourier synthesis.) The maximum in the SLD profile for the headgroup-deuterated CHOL is located 22.9 ± 0.2 Å from the unit cell center. This leaves a distance of 4 Å between the headgroup position and the unit cell boundary. The maximum of the peak for the deuterated CHOL tail was located 6.2 ± 0.2 Å (both CHOL head and tail position were determined by Gaussian peak fitting of the corresponding peaks) from the center of the unit cell. Such an arrangement of the CHOL molecules within the SPP unit cell will allow van der Waals interactions between the cholestane rings and the CER and FFA acyl chains, and hydrogen bonding between the sterol hydroxyl group and the CERs and/or the carbonyl groups of the FFAs.

Interdigitation of FFA and CER

When focusing on the SLD profiles for the systems containing perdeuterated and hydrogenous FFA, it may be noted that the former—as would be expected—is shifted to a higher mean SLD compared with the latter, but that there is also a significantly elevated density at the center of the unit cell. This elevated density is attributed to a partial interdigitation of the FFA acyl chains (see Fig. 4 *C*)—an arrangement that is consistent with the fact that the SPP has a repeat spacing of 53.9 ± 0.3 Å while two opposing C24 chains arranged perpendicular to the basal plane would result in a repeating unit of 60 Å. This arrangement is very similar to that seen for CER NS, the acyl chains of which were also found to interdigitate in the SPP unit cell (32). Based on previous studies, it has been proposed that the CERs dictate the length of the unit cell (23,28,46), and this may also be true for the systems studied here.

The role of CHOL in the SPP unit cell

In our mixture, 86 mol % of the FFAs have a chain length beyond that of C20 (long-chain FFA), and only 13.5 mol % of the FFAs have a chain length of up to and including C20 (short-chain FFA). The proportion of short-chain FFAs present is insufficient to fill the voids in the bilayer opposite the long-chain FFAs and the C24 acyl chain of CERs that extend beyond the unit cell center. The other candidate

components for opposing the long-chain FFAs are CHOL and CER NP C16. The results obtained here demonstrate that the CHOL is not present at the center of the unit cell but located 6.2 ± 0.2 Å away from the center. This is at approximately the same position in the bilayer as the tail-end of the short-chain FFAs and the C18 sphingoid base of the CERs. The latter compensate for the C24 acyl chain of the CERs. Therefore, it seems that the role of CHOL is to compensate for the extension of the long-chain FFAs being beyond the center of the bilayer. As the interfacial area per CHOL molecule is approximately twice that of a FFA, each CHOL molecule can compensate two long-chain FFA molecules (47–50). Recently we observed that the minimum CHOL level required for the formation of the SPP is ~20 mol % (E.H. Mojumdar, G.S. Gooris, and J.A. Bouwstra, unpublished data). This is approximately the level of CHOL that is required to compensate for the long-chain FFAs that cannot be compensated by the short-chain FFAs that are present at a much lower level.

Molecular model of the SPP

Based on the positions within the SPP unit cell determined here for CHOL and FFA, and the CER NS position determined in our earlier experiments (32) a molecular model is proposed for the SPP lipid model system (Fig. 4 *C*). In the proposed model, the CER NS molecules are shown in a symmetric hairpin arrangement. However, due to the resolution of the Fourier synthesis and the small intermembrane space between the lipid headgroups as was previously reported, it is impossible, using our data, to distinguish between a fully extended and a hairpin arrangement of the CERs (32). Therefore, both arrangements are, in principle, still possible. The experimental results we obtained using synthetic lipid materials are in accordance with the theoretical simulation studies of SC lipid mixtures where it was shown that CER NS shows significant interdigitation at the center of the unit cell, and with the CHOL headgroups located close to the water-lipid interface (51,52).

Synthetic samples

For synthetic samples, the signal/noise of our measurements is quite low. As a result, a large amount of material and longer measurement times are required to achieve a sufficient signal/noise. Unlike phospholipid systems that can incorporate 12–35 water molecules (38), our synthetic model membranes show low levels of hydration, and thereby mimic the situation in natural SC. The most likely reason for this is the formation of hydrogen bondings between the CER headgroups (53–55). The poor hydration level explains the lack of swelling in our model membrane systems (32). For calculation of the scattering length density profiles for different lipid model systems, the structure factors at 8% D_2O have been used. In the case of 8% D_2O, the water has a net zero neutron scattering length density (56). In this situation, small structural details of the lipid lamellae can be well observed.

CONCLUSIONS

Our data unequivocally show the CHOL and FFA positions within the unit cell of the SPP. Together with the CER NS arrangement published recently (32), these data provide detailed information about the molecular architecture of the SPP in our lipid model, mimicking closely the lamellae present in human SC. The SC also involves the LPP phase, however, and this greatly contributes to the skin barrier. Therefore, to obtain a fuller picture of the SC structure, it is of interest to investigate the molecular arrangement of the various lipid components within the LPP unit.

SUPPORTING MATERIAL

Four figures and a subsection called Determining the Water Phase Signs are available at http://www.biophysj.org/biophysj/supplemental/S0006-3495(13)00782-0.

We thank the company Cosmoferm (Evonik) for their generous provision of CERs and the Institut Laue-Langevin for the allocation of beam time for neutron diffraction analysis.

REFERENCES

1. Wertz, P. W., and B. van den Bergh. 1998. The physical, chemical and functional properties of lipids in the skin and other biological barriers. *Chem. Phys. Lipids.* 91:85–96.
2. Boddé, H. E., I. van den Brink, …, F. H. N. de Haan. 1991. Visualization of in vitro percutaneous penetration of mercuric chloride; transport through intercellular space versus cellular uptake through desmosomes. *J. Control. Release.* 15:227–236.
3. Talreja, P., N. K. Kleene, …, G. B. Kasting. 2001. Visualization of the lipid barrier and measurement of lipid pathlength in human *stratum corneum*. *AAPS PharmSci.* 3:E13.
4. Elias, P. M. 1983. Epidermal lipids, barrier function, and desquamation. *J. Invest. Dermatol.* 80(*Suppl*):4s–49s.
5. Weerheim, A., and M. Ponec. 2001. Determination of *stratum corneum* lipid profile by tape stripping in combination with high-performance thin-layer chromatography. *Arch. Dermatol. Res.* 293:191–199.
6. Gray, G. M., and R. J. White. 1978. Glycosphingolipids and ceramides in human and pig epidermis. *J. Invest. Dermatol.* 70:336–341.
7. Yardley, H. J., and R. Summerly. 1981. Lipid composition and metabolism in normal and diseased epidermis. *Pharmacol. Amp. Ther.* 13:357–383.
8. Gray, G. M., and H. J. Yardley. 1975. Different populations of pig epidermal cells: isolation and lipid composition. *J. Lipid Res.* 16:441–447.
9. Holleran, W. M., M. Q. Man, …, K. R. Feingold. 1991. Sphingolipids are required for mammalian epidermal barrier function. Inhibition of sphingolipid synthesis delays barrier recovery after acute perturbation. *J. Clin. Invest.* 88:1338–1345.
10. Coderch, L., O. López, …, J. L. Parra. 2003. Ceramides and skin function. *Am. J. Clin. Dermatol.* 4:107–129.
11. van Smeden, J., L. Hoppel, …, J. A. Bouwstra. 2011. LC/MS analysis of *stratum corneum* lipids: ceramide profiling and discovery. *J. Lipid Res.* 52:1211–1221.

12. Wertz, P. W., M. C. Miethke, …, D. T. Downing. 1985. The composition of the ceramides from human *stratum corneum* and from comedones. *J. Invest. Dermatol.* 84:410–412.

13. Ponec, M., A. Weerheim, …, P. Wertz. 2003. New acylceramide in native and reconstructed epidermis. *J. Invest. Dermatol.* 120:581–588.

14. Masukawa, Y., H. Narita, …, K. Kita. 2008. Characterization of overall ceramide species in human *stratum corneum*. *J. Lipid Res.* 49:1466–1476.

15. White, S. H., D. Mirejovsky, and G. I. King. 1988. Structure of lamellar lipid domains and corneocyte envelopes of murine *stratum corneum*. An x-ray diffraction study. *Biochemistry.* 27:3725–3732.

16. Bouwstra, J. A., G. S. Gooris, …, W. Bras. 1991. Structural investigations of human *stratum corneum* by small-angle x-ray scattering. *J. Invest. Dermatol.* 97:1005–1012.

17. Cornwell, P. A., B. W. Barry, …, J. A. Bouwstra. 1994. Wide-angle x-ray diffraction of human *stratum corneum*: effects of hydration and terpene enhancer treatment. *J. Pharm. Pharmacol.* 46:938–950.

18. Ohta, N., S. Ban, …, I. Hatta. 2003. Swelling of intercellular lipid lamellar structure with short repeat distance in hairless mouse *stratum corneum* as studied by x-ray diffraction. *Chem. Phys. Lipids.* 123:1–8.

19. Hatta, I., N. Ohta, …, N. Yagi. 2006. Coexistence of two domains in intercellular lipid matrix of *stratum corneum*. *Biochim. Biophys. Acta Biomembr.* 1758:1830–1836.

20. Bouwstra, J. A., G. S. Gooris, …, M. Ponec. 1996. Phase behavior of isolated skin lipids. *J. Lipid Res.* 37:999–1011.

21. Bouwstra, J. A., G. S. Gooris, …, M. Ponec. 2001. Phase behavior of lipid mixtures based on human ceramides: coexistence of crystalline and liquid phases. *J. Lipid Res.* 42:1759–1770.

22. de Jager, M. W., G. S. Gooris, …, J. A. Bouwstra. 2004. Novel lipid mixtures based on synthetic ceramides reproduce the unique *stratum corneum* lipid organization. *J. Lipid Res.* 45:923–932.

23. de Jager, M. W., G. S. Gooris, …, J. A. Bouwstra. 2004. Modeling the *stratum corneum* lipid organization with synthetic lipid mixtures: the importance of synthetic ceramide composition. *Biochim. Biophys. Acta Biomembr.* 1664:132–140.

24. de Jager, M. W., G. S. Gooris, …, J. A. Bouwstra. 2005. Lipid mixtures prepared with well-defined synthetic ceramides closely mimic the unique *stratum corneum* lipid phase behavior. *J. Lipid Res.* 46:2649–2656.

25. Kiselev, M. A., N. Y. Ryabova, …, R. H. Neubert. 2005. New insights into the structure and hydration of a *stratum corneum* lipid model membrane by neutron diffraction. *Eur. Biophys. J.* 34:1030–1040.

26. de Jager, M., W. Groenink, …, J. Bouwstra. 2006. Preparation and characterization of a *stratum corneum* substitute for in vitro percutaneous penetration studies. *Biochim. Biophys. Acta Biomembr.* 1758:636–644.

27. Groen, D., G. S. Gooris, …, J. A. Bouwstra. 2008. Two new methods for preparing a unique *stratum corneum* substitute. *Biochim. Biophys. Acta Biomembr.* 1778:2421–2429.

28. Groen, D., G. S. Gooris, and J. A. Bouwstra. 2009. New insights into the *stratum corneum* lipid organization by x-ray diffraction analysis. *Biophys. J.* 97:2242–2249.

29. McIntosh, T. J. 2003. Organization of skin *stratum corneum* extracellular lamellae: diffraction evidence for asymmetric distribution of cholesterol. *Biophys. J.* 85:1675–1681.

30. Ruettinger, A., M. A. Kiselev, …, R. H. Neubert. 2008. Fatty acid interdigitation in *stratum corneum* model membranes: a neutron diffraction study. *Eur. Biophys. J.* 37:759–771.

31. Schröter, A., D. Kessner, …, R. H. H. Neubert. 2009. Basic nanostructure of *stratum corneum* lipid matrices based on ceramides [EOS] and [AP]: a neutron diffraction study. *Biophys. J.* 97:1104–1114.

32. Groen, D., G. S. Gooris, …, J. A. Bouwstra. 2011. Disposition of ceramide in model lipid membranes determined by neutron diffraction. *Biophys. J.* 100:1481–1489.

33. Wertz, P. W., and D. T. Downing. 1991. Epidermal lipids. *In* Physiology, Biochemistry, and Molecular Biology of the Skin. L. A. Goldsmith, editor. Oxford University Press, New York, pp. 205–236.

34. Richard, D. 2008. http://www.ill.eu/instruments-support/computing-for-science/data-analysis/. Accessed May 2010.

35. Franks, N. P., and W. R. Lieb. 1979. The structure of lipid bilayers and the effects of general anesthetics. An x-ray and neutron diffraction study. *J. Mol. Biol.* 133:469–500.

36. NIST Center for Neutron Research. 2005. www.ncnr.nist.gov/instruments/bt1/neutron.html. Accessed May 2010.

37. Worcester, D. L., and N. P. Franks. 1976. Structural analysis of hydrated egg lecithin and cholesterol bilayers. II. Neutrol diffraction. *J. Mol. Biol.* 100:359–378.

38. Nagle, J. F., and S. Tristram-Nagle. 2000. Structure of lipid bilayers. *Biochim. Biophys. Acta. Rev. Biomembr.* 1469:159–195.

39. Harroun, T. A., J. Katsaras, and S. R. Wassall. 2006. Cholesterol hydroxyl group is found to reside in the center of a polyunsaturated lipid membrane. *Biochemistry.* 45:1227–1233.

40. NIST Center for Neutron Research. 2010. http://www.ncnr.nist.gov/resources/sldcalc.html. Accessed January 2011.

41. Wiener, M. C., G. I. King, and S. H. White. 1991. Structure of a fluid dioleoylphosphatidylcholine bilayer determined by joint refinement of x-ray and neutron diffraction data. I. Scaling of neutron data and the distributions of double bonds and water. *Biophys. J.* 60:568–576.

42. Wiener, M. C., and S. H. White. 1991. Fluid bilayer structure determination by the combined use of x-ray and neutron diffraction. II. "Composition-space" refinement method. *Biophys. J.* 59:174–185.

43. Jacobs, R. E., and S. H. White. 1989. The nature of the hydrophobic binding of small peptides at the bilayer interface: implications for the insertion of transbilayer helices. *Biochemistry.* 28:3421–3437.

44. Kanicky, J. R., and D. O. Shah. 2002. Effect of degree, type, and position of unsaturation on the pK_a of long-chain fatty acids. *J. Colloid Interface Sci.* 256:201–207.

45. Kučerka, N., D. Marquardt, …, J. Katsaras. 2009. The functional significance of lipid diversity: orientation of cholesterol in bilayers is determined by lipid species. *J. Am. Chem. Soc.* 131:16358–16359.

46. Bouwstra, J. A., G. S. Gooris, …, M. Ponec. 1998. Role of ceramide 1 in the molecular organization of the *stratum corneum* lipids. *J. Lipid Res.* 39:186–196.

47. El-Hefian, E. A. 2009. Surface investigation of chitosan film with fatty acid monolayers. *Maejo Int. J. Sci. Technol.* 3:277.

48. Shaitan, K. V., and P. P. Pustoshilov. 1999. Molecular dynamics of a stearic acid monolayer. *Biophysics.* 44:429–434 [Translated from Biofizika. 44:436–441].

49. Hofsäss, C., E. Lindahl, and O. Edholm. 2003. Molecular dynamics simulations of phospholipid bilayers with cholesterol. *Biophys. J.* 84:2192–2206.

50. Shieh, H.-S., L. G. Hoard, and C. E. Nordman. 1981. The structure of cholesterol. *Acta Crystallogr. B.* 37:1538–1543.

51. Das, C., M. G. Noro, and P. D. Olmsted. 2009. Simulation studies of *stratum corneum* lipid mixtures. *Biophys. J.* 97:1941–1951.

52. Hoopes, M. I., M. G. Noro, …, R. Faller. 2011. Bilayer structure and lipid dynamics in a model *stratum corneum* with oleic acid. *J. Phys. Chem. B.* 115:3164–3171.

53. Moore, D. J., M. E. Rerek, and R. Mendelsohn. 1999. Role of ceramides 2 and 5 in the structure of the *stratum corneum* lipid barrier. *Int. J. Cosmet. Sci.* 21:353–368.

54. Rerek, M. E., B. Chen, …, D. J. Moore. 2001. Phytosphingosine and sphingosine ceramide headgroup hydrogen bonding: structural insights through thermotropic hydrogen/deuterium exchange. *J. Phys. Chem. B.* 105:9355–9362.

55. Moore, D. J. ., and M. E. Rerek. 2000. Insight into the molecular organization of lipids in the skin barrier from infrared spectroscopy studies of *stratum corneum* lipid models. *Acta Derm. Venereol.* 208:16–22.

56. Kučerka, N., D. Marquardt, …, J. Katsaras. 2010. Cholesterol in bilayers with PUFA chains: doping with DMPC or POPC results in sterol reorientation and membrane-domain formation. *Biochemistry.* 49:7485–7493.